Dijet Production from $\overline{p}p$ Collisions at 1.8 TeV

Alfred T. Goshaw
Duke University, Physics Department, Box 90305, Durham, NC 27708, USA

For the CDF Collaboration
The production properties of dijets from $\overline{p}p$ collisions at $\sqrt{s} = 1.8$ TeV have been studied using the Collider Detector at Fermilab. This report presents an analysis of the dijet angular distributions using 106 pb^{-1} of data collected during Run I of the Tevatron Collider. The measured angular distributions agree with next-to-leading order QCD predictions in five dijet invariant mass regions with average dijet mass varying from 263 to 698 GeV/c^2. The predicted angular distributions are relatively insensitive to parton distribution functions, and therefore these data can be used to put limits on energy scale parameters used to describe contact interactions. For a model with only up and down quarks composite, the data exclude at 95% confidence level a contact interaction scale $\Lambda^+_{ud} \leq 1.6$ TeV or $\Lambda^-_{ud} \leq 1.4$ TeV.

1 Introduction

One of the most fundamental processes occurring in high energy $\overline{p}p$ collisions is the production of dijets. These events can be used to test the QCD sector of the Standard Model and to sensitively search for new physics occurring at small distance scales. This could take the form of massive new particles decaying to dijets or the appearance of a short range contact interaction. This report presents the results of a measurement of the dijet production angular distribution and makes a comparison to the predictions of next-to-leading order (NLO) perturbative QCD. The QCD predictions for the dijet angular distribution is fairly insensitive to parton distributions and jet clustering methods, and therefore provides a good test of perturbative QCD calculations at the matrix element level.

In the analysis presented here, the production dynamics is studied in terms of two variables which are kinematically orthogonal: the dijet mass M and a variable χ related to the dijet center of mass production angle θ^*. If the dijets are produced from the fragmentation of partons produced from a 2 to 2 scattering process, the production dynamics can be described in terms of the standard Mandelstam variables $\hat{s}$, $\hat{t}$ and $\hat{u}$, only two of which are independent. $\hat{s}$ is determined from the invariant mass of the two jets: $M = \sqrt{(E_1+E_2)^2 - (\vec{P}_1+\vec{P}_2)^2}$. For the second Lorentz invariant variable we define $\chi = \hat{u}/\hat{t}$. χ appears naturally as a parameter in the QCD matrix element and also can be measured well experimentally. If the partons are massless, χ

is simply related to the parton-parton center of mass scattering angle θ^* and to the pseudorapidity of the partons η^*: $\chi = (1 + |\cos\theta^*|)/(1 - |\cos\theta^*|) = \exp(|\eta_1^* - \eta_2^*|)$. Distributions in θ^* and χ obviously carry the same information, but for QCD production processes the χ distribution tends to be relatively flat and is therefore a more convenient variable to use. Also, neglecting the transverse momentum of the parton-parton system relative to the $\overline{p}p$ collision axis, the pseudorapidity difference is invariant under boosts to the $\overline{p}p$ center of mass, and χ can be measured as $\exp(|\eta_1 - \eta_2|)$ from the pseudorapidity difference between the jets as measured directly in the laboratory. This makes the measurement of χ relatively insensitive to jet E_t corrections and to jet clustering algorithms.

For the analysis presented here we study the dijet production angular distribution in terms of χ as measured from the leading jets which are selected as defined below. The distributions in χ are compared to the predictions of NLO QCD calculations for the five different dijet mass ranges tabulated in Table 1. These data are then used to extract limits on energy scale parameters used to characterize left-handed contact interactions.

2 Selection of Dijet Events

The data are taken from $\overline{p}p$ collisions at $\sqrt{s} = 1.8$ TeV as measured using the Collider Detector at Fermilab (CDF). A total of 106 pb^{-1} of integrated luminosity is used for this analysis. A detailed description of the CDF detector can be found elsewhere [1]. Jets are reconstructed in calorimeters which cover a pseudorapidity range out to $\eta = 2.7$. The jets are clustered using calorimeter towers inside a radius $R = \sqrt{(\Delta\eta)^2 + (\Delta\phi)^2} = 0.7$ centered on an E_T weighted $\eta - \phi$ centroid of calorimeter towers. Corrections are made for non-linearities in the calorimeter response, energy loss in uninstrumented regions and outside the clustering cone, and energy gained from the underlying event and multiple primary $\overline{p}p$ collisions within a bunch crossing. The jet energy corrections increase the detected jet energies by 24% to 19% as the jet energies increase from 50 to 500 GeV. Details of jet reconstruction and energy corrections are described elsewhere [2].

The data used for this analysis were selected using single jet triggers with thresholds on the uncorrected transverse energy set at 20, 50, 70 and 100 GeV. In order to limit the online data rates the three lower threshold triggers were prescaled, resulting in four data samples with integrated luminosities 0.126, 2.84, 14.1, and 106 pb^{-1} . The transverse energy of the jets in an event were corrected for instrumental effects as described above, and the dijet system selected as the two highest Et (leading) jets. The leading jets were also required

Table 1: Dijet events used for the angular distribution analysis. The units of mass are GeV/c^2. Also shown are the measured values of the angular ratio R_χ as defined in the text.

Dijet Mass Range	$< Mass >$	Number of Events	R_χ	Stat.	Sys.
241 to 300	263	15023	0.678	0.012	0.018
300 to 400	334	23227	0.695	0.010	0.025
400 to 517	440	28202	0.703	0.009	0.033
517 to 625	557	4425	0.738	0.023	0.054
over 625	698	1056	0.732	0.046	0.103

to have pseudorapidities in the range -2.0 to +2.0 to insure that the jets were well measured. The 20 GeV trigger sample was used to measure the efficiency of the 50 GeV trigger, and the 50, 70 and 100 GeV triggers were used to select dijets with invariant mass greater than 241, 300 and 400 GeV/c^2. Using these selection criteria the trigger efficiencies are greater than 95 % for the dijets used to measure the angular distributions in the range χ=1.0 (θ^*=90^o) to χ=5.0 (θ^*=48^o or 132^o).

A cleanup of the data sample rejects events with a $\overline{p}p$ collision vertex over 60 cm from the center of the detector, and suppresses backgrounds due to cosmic rays, beam halo and detector noise by removing events with missing Et significance greater than 6, and sum of the transverse or total observed energy in the event greater than 2 TeV [3].

3 The Dijet Production Angular Distribution

The final dijet event sample used for the angular distribution measurements consists of 71933 dijets, distributed into the five invariant mass bins shown in Table 1. The variation in dijet mass response and resolution as a function of detector η produced distortions in the measured angular distribution. The relative jet response was determined using the technique of P_T balance: fixing a jet in the region $0.15 < |\eta| < 0.9$ and measuring the relative response of a jet in another pseudorapidity region. For example at $M > 625$ GeV/c^2, a 6% larger jet response at $|\eta| < 0.15$ and a 4% smaller jet response at $0.9 < |\eta| < 1.4$, produced a tilt in the angular distribution which increased the relative rate at $\chi = 1$ by about 10% and lowered the relative rate at $\chi = 5$ by about 10%. The fully corrected χ distributions in each of the five dijet mass regions are plotted in Figure 1 and tabulated in Table 2.

Table 2: The dijet angular distribution and statistical uncertainty for the five mass bins (GeV/c^2).

	(100/N)(dN/dχ)				
χ	$241 < M < 300$	$300 < M < 400$	$400 < M < 517$	$517 < M < 625$	$M > 625$
1.25	31.1 ± 0.7	31.7 ± 0.5	31.9 ± 0.5	32.6 ± 1.2	31.7 ± 2.4
1.75	26.8 ± 0.6	26.5 ± 0.5	26.3 ± 0.4	27.2 ± 1.1	26.5 ± 2.2
2.25	23.0 ± 0.6	23.8 ± 0.5	24.3 ± 0.4	25.1 ± 1.1	26.3 ± 2.2
2.75	23.4 ± 0.6	23.2 ± 0.5	23.9 ± 0.4	23.0 ± 1.0	25.3 ± 2.2
3.25	24.3 ± 0.7	23.8 ± 0.5	23.5 ± 0.4	21.2 ± 1.0	21.6 ± 2.0
3.75	22.5 ± 0.6	24.0 ± 0.5	23.3 ± 0.4	24.1 ± 1.1	22.2 ± 2.1
4.25	24.6 ± 0.8	23.3 ± 0.5	23.6 ± 0.5	22.8 ± 1.1	22.4 ± 2.1
4.75	24.4 ± 0.8	23.7 ± 0.5	23.1 ± 0.5	24.1 ± 1.2	24.0 ± 2.2

4 Comparison to QCD Predictions

We have compared the data to parton level predictions of leading order (LO) QCD and next to leading order (NLO) QCD [4]. The LO calculations use CTEQ2L parton distributions, and the NLO QCD calculation uses CTEQ2M parton distributions [5]. Many alternate parton distribution sets were tried, including one in which the gluon distribution of the proton was significantly increased[6], and the calculations were insensitive to the choice of parton distribution. Fig. 1 shows the data compared to the LO (dashed) and NLO (solid) QCD predictions. The distributions in χ are well reproduced by the QCD predictions in all five mass regions.

In order to characterize the shape of the angular distribution in a mass bin with a single number, we use the angular variable $R_\chi = N(\chi < 2.5)/N(2.5 < \chi < 5)$ the ratio of the number of dijets with $\chi < 2.5$ to the number of dijets with $2.5 < \chi < 5$. For R_χ the acceptance corrections reduce raw R_χ by 1%, 2%, 3%, 5% and 6% for the 5 mass bins respectively. The corrections increase with mass because the spectrum is steeper at higher mass, leading to a larger distortion of the angular distribution. The measured values of R_χ are plotted in Fig. 2 and tabulated in Table 1. In Fig. 2 the QCD predictions for R_χ are shown for two different choices of renormalization scale, $\mu = M$ and $\mu = P_T$. Note that the renormalization scale dependence of the NLO calculation is significantly less than that of the LO calculation, and estimates the precision of the NLO QCD calculation. The systematic uncertainties, shown only in Fig. 2 and Table 2, arise from the uncertainty in the jet energy response as a function of η. The dominant response uncertainties were in the region $0.0 < |\eta| < 0.15$ (between 3% and 6%) and the region $0.9 < |\eta| < 1.4$ (4%). Other systematic uncertainties are negligible in comparison.

The angular distributions and angular ratio are in good agreement with the NLO QCD prediction and do not require the presence of new physics. The data prefer the NLO QCD prediction with renormalization scale $\mu = P_t$ with a $\chi^2 = 8.36$ for 5 degrees of freedom, taking into account the correlated systematic errors. This is significantly better than $\chi^2 = 13.1$ for NLO QCD with $\mu = M$.

5 Addition of a Contact Interaction to the QCD Prediction

In order to quantitatively evaluate the sensitivity of the dijet data to new physics we chose a simple model in which a left-handed contact interaction is added to the LO QCD prediction. The Lagrangian describing the contact interaction depends on an energy scale parameter Λ, the sign of the interference term with the LO QCD prediction (+ or -), and assumptions about how many of the quarks have compositeness modeled by the contact interaction. For the quark compositeness we consider two cases: u and d quarks only [7] or the flavor symmetric case with u,d,s,c and b quarks composite [8]. The LO QCD plus contact interaction predictions are normalized to equal the NLO QCD prediction with renormalization scale $\mu = P_T$ when the contact scale is $\Lambda = \infty$. This was done by multiplying the LO QCD plus contact interaction predictions by the ratio of the NLO to LO QCD predictions.

Using this method, the predictions for LO QCD plus contact interactions can be compared to the measured χ and R_χ distributions. For example, Fig. 1 shows the prediction of a contact term with u and d quarks composite and an energy scale parameter $\Lambda^+_{ud} = 1.6$ TeV. This illustrates the increasing sensitivity of the dijet angular distribution to the contact interaction as the dijet mass increases, thus probing decreasing length scales. Compositeness predictions for the R_χ distribution are shown in Fig. 2 for energy scales ranging from 1.4 to 1.8 TeV in a model with u and d quarks composite.

We use the measured R_χ distribution to put limits on the contact interaction in terms of the energy scale parameter Λ. A statistical comparison between the data and the theory is made from the inverse of the variance matrix, $(V^{-1})_{ij}$, and the difference between the data and the theory in each bin, Δ_i. Using the standard relation in which repeated indices are summed the $\chi^2 = \Delta_i (V^{-1})_{ij} \Delta_j$. This properly takes into account the statistical and fully correlated systematic errors tabulated in Table 1. The 95% CL excluded contact interaction occurs where the χ^2 has increased from the QCD value to greater than 11.0. In a model of contact interactions where the up and down type quarks are composite we exclude at 95% CL the scales $\Lambda^+_{ud} \leq 1.6$ TeV and $\Lambda^-_{ud} \leq 1.4$. For flavor symmetric contact interactions among all quarks [8], not just u and d quark, the scales excluded by the angular distributions are $\Lambda^+ \leq 1.8$ TeV and $\Lambda^- \leq 1.6$ TeV.

6 Conclusions

We have measured the dijet angular distributions and found them to be in good agreement with NLO QCD for five dijet mass regions ranging from a low of $< Mass > = 263$ GeV/c^2 to a high of $< Mass > = 698$ GeV/c^2. The data have been used to put limits on new physics as modeled by left-handed contact interactions. In a specific model of a contact interaction where the up and down quarks are composite we exclude at a 95% CL the scales $\Lambda^+_{ud} \leq 1.6$ TeV and $\Lambda^-_{ud} \leq 1.4$.

Acknowledgments

We thank the Fermilab staff and the technical staffs of the participating institutions for their vital contributions. This work was supported by the U.S. Department of Energy and National Science Foundation; the Italian Istituto Nazionale dijets Fisica Nucleare; the Ministry of Science, Culture, and Education of Japan; the Natural Sciences and Engineering Research Council of Canada; the A. P. Sloan Foundation; and the Alexander von Humboldt-Stiftung.

References

1. F. Abe et al., Nucl. Inst. and Meth. **A271**, 387 (1988).
2. F. Abe et al., Phys. Rev. **D45**, 1448 (1992).
3. F. Abe et al., Phys. Rev. Lett. **74**, 3538, (1995).
4. JETRAD from W. Giele et al., Phys. Rev. Lett. 73, 2019 (1994).
5. J. Botts et al., Phys. Lett. **B304**, 159 (1993).
6. J. Huston et al., MSU-HEP-50812, hep-ph/9511386.
7. E. Eichten, K. Lane and M. Peskin, Phys. Rev. Lett. **50**, 811 (1983).
8. K. Lane, BUHEP-96-8, hep-ph/9605257.

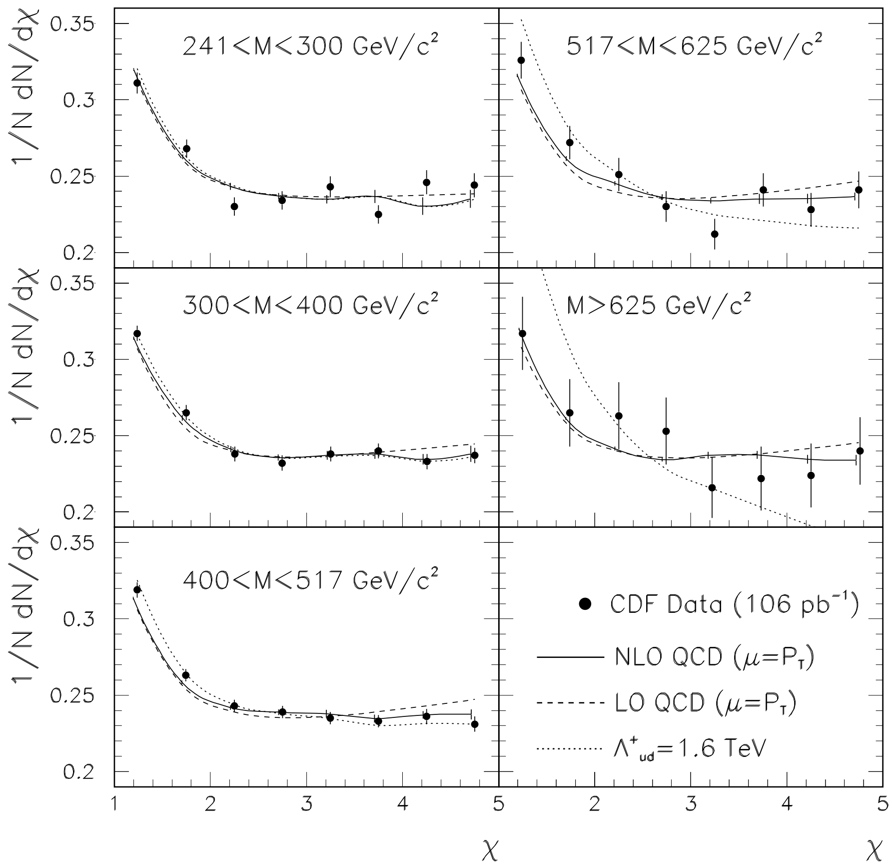

Figure 1: The dijet angular distribution (points) compared to predictions of NLO QCD (solid), LO QCD (dashes), and LO QCD with a quark contact interaction (dots). The contact interaction calculation is normalized to equal NLO QCD when $\Lambda = \infty$. Error bars on the data and NLO QCD are statistical.

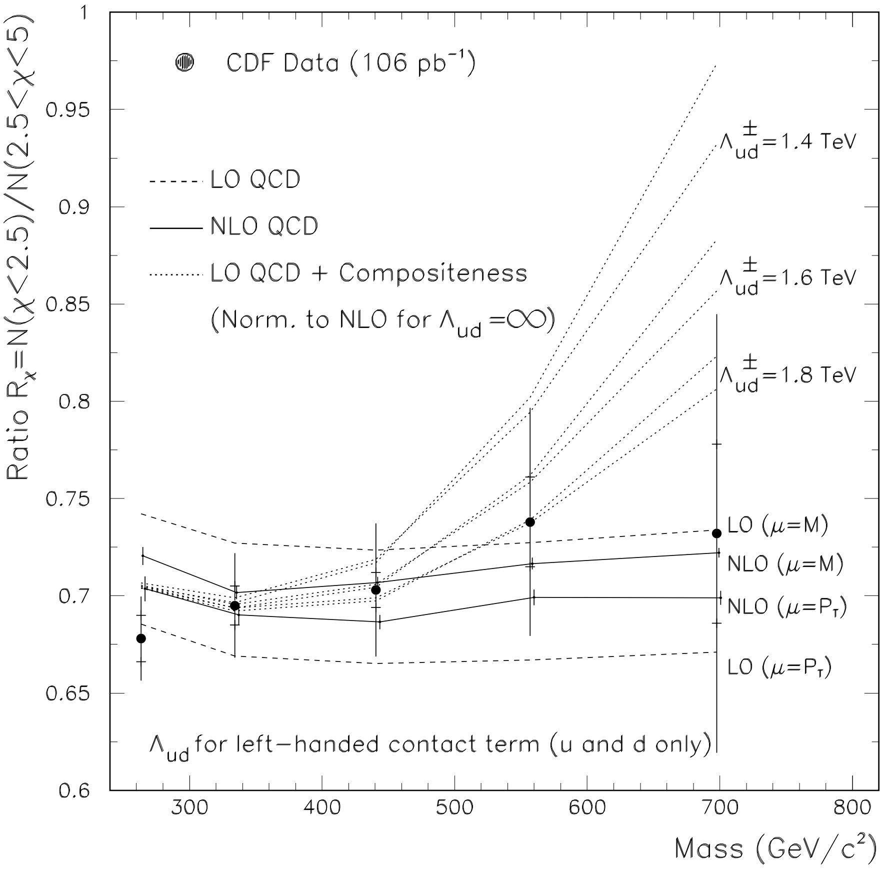

Figure 2: The dijet angular ratio (points) compared to LO QCD (dashed), NLO QCD (solid), and LO QCD + quark contact interaction normalized to NLO at $\Lambda_{ud} = \infty$ (dots). QCD is shown for two renormalization scales ($\mu = M$ and $\mu = P_T$). Contact interactions are displayed for three different compositeness scales, with two different signs for the amplitude of the contact term (upper dotted curve is Λ^+, lower dotted curve is Λ^-). The inner error bars on the data are statistical uncertainties and the outer error bars are statistical and systematic uncertainties added in quadrature. The error bars on NLO QCD are statistical.